

Chapter 6—Kinetics of HO₂ + HCHO and Further Reaction of the Hydroxymethylperoxy Radical (HOCH₂OO•)

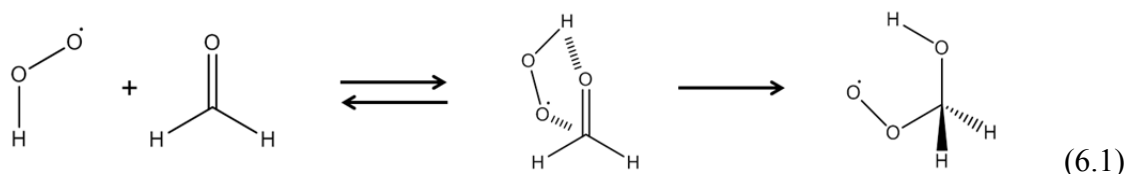
Abstract

In Chapters 4 and 5, we presented and assigned the ν_1 and A-X spectra of the isomerization product of HO₂ + HCHO: the hydroxymethylperoxy radical (HOCH₂OO•, HMP). Based on our chemistry analysis, the observed bands are unique to HMP (early times only for ν_1 , all times for A-X). In this thesis chapter, we use the ν_1 and A-X cavity ringdown spectra of HMP to measure its formation (HO₂ + HCHO) and destruction kinetics. We determine the rate constant $k_{\text{HO}_2+\text{HCHO}}$ by measuring the ν_1 absorption as a function of time under pseudo first order conditions ($[\text{HCHO}] \gg [\text{HO}_2]$). Destruction of HMP is monitored by measuring the A-X absorptions as a function of time and comparing to a kinetics model using existing rate constants. Using the ν_1 band, we report $k_{\text{HO}_2+\text{HCHO}} = (4.8 \pm 1.7) \times 10^{-14} \text{ cm}^3 \text{ molec}^{-1} \text{ s}^{-1}$ (2σ), in excellent agreement with previous studies. Our A-X study gives an HMP destruction rate in agreement with the existing kinetics model (for our conditions, lifetime 1 ms). These results indicate that the previous end-product and B-X (contaminated spectra) studies were able to model secondary chemistry and subtract out contaminations quite well.

The methods described in Chapters 4-6 can be readily extended to the HO₂ + acetone system: directly detecting 2-hydroxyisopropylperoxy (2-HIPP). We show in this chapter that in order to carry out CRDS measurements on 2-HIPP, we need to cool our kinetics cell to 190–250 K, depending on the exact equilibrium constant for the HO₂ + acetone reaction.

Introduction

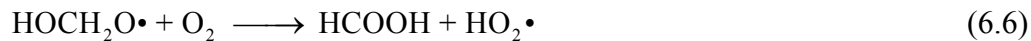
Let us begin with a summary of what we have learned about $\text{HO}_2 + \text{HCHO}$ so far from our CRDS and quantum chemistry studies. Our spectroscopy studies in Chapter 4 support the current understanding of the $\text{HO}_2 + \text{HCHO}$ reaction (Reaction 6.1): formation of a complex followed by isomerization to form the hydroxymethylperoxy radical ($\text{HOCH}_2\text{OO}\cdot$, or HMP).



We have detected both the ν_1 (OH stretch) vibrational band of HMP, and the A-X electronic transition characteristic of all peroxy radicals. The intensities,¹²² positions, shapes of these spectroscopic bands are consistent with our quantum chemistry calculations (Chapter 5). Additionally, the chemistry analysis presented in Chapter 4 indicates that under our experimental conditions, our spectra are dominated by HMP. With all of these pieces of data, we are confident that our spectra can be assigned to HMP.

We now turn our attention to the kinetics of HMP: both formation (Reaction 6.1) and destruction (Reactions 6.2–6.6). The main destruction pathways of HMP are reaction with HO_2 (Reactions 6.2 and 6.3) or self-reaction (Reactions 6.4 and 6.5). Termination of Reaction 6.5 ($\text{HOCH}_2\text{O}\cdot$) occurs by reaction with O_2 .





Previous studies have measured the kinetics of HMP formation and destruction either by end-product analysis^{24, 99} or by direct measurement via the B-X band in the UV.^{25, 26} These two methods each come with their own set of problems. Any end-product study must make assumptions about the rest of the kinetics model in order to derive a rate constant for the reaction of interest ($\text{HO}_2 + \text{HCHO}$), subjecting $k_{\text{HO}_2+\text{HCHO}}$ (or other rate constants) to large uncertainties. The kinetics as measured by the B-X bands required corrections for other chemical species, notably HCOOH, which forms in large quantities over the timescales used for the previous experiments (1 s).^{25, 26}

We can use the spectroscopic bands of HMP from Chapter 4 to measure the kinetics of Reactions 6.1-6.6. Under the correct conditions, both of these bands (ν_1 , A-X) will provide direct detection and unique measures of HMP. Each spectroscopic band carries its own advantages and disadvantages. The ν_1 band is unique to HMP at early times (shown in Chapter 4, Figure 4.2) and is very strong ($\sigma = 10^{-19} \text{ cm}^2 \text{ molec}^{-1}$), making it ideal for measuring the formation rate of HMP ($k_{\text{HO}_2+\text{HCHO}}$, Reaction 6.1). However, as observed from Reactions 6.2–6.6, other ν_1 bands (HOCH_2OOH , $\text{HOCH}_2\text{O}\cdot$, HCOOH) will interfere with the spectrum at later times, making measurements of HMP destruction impossible. Conversely, the A-X bands are weak ($\sigma = 10^{-21} \text{ cm}^2 \text{ molec}^{-1}$), making measurements of $k_{\text{HO}_2+\text{HCHO}}$ difficult due to the fast rise time of the HMP absorption. Because the A-X bands are unique measures of HMP, these bands are well-suited for making measurements of the relatively slow HMP destruction (lifetime 1 ms under our conditions, as shown in Chapter 4).

In our spectroscopy study, we made use of a large excess of [HCHO] (a factor of 30–1000 greater than [HO₂]), in effect keeping [HCHO] constant during the experiment. By using similar conditions in our kinetics study, we can obtain pseudo-first-order kinetics when analyzing the HMP formation (Reaction 6.1).

This thesis chapter describes the first kinetics measurements on HMP formation and destruction as measured via the ν_1 vibrational and A-X electronic bands of HMP. Similar to the experiments in Chapter 4, HMP was generated by pulsed laser photolysis of Cl₂ in the presence of formaldehyde and O₂. Cavity ringdown spectroscopy was used to measure the formation and destruction of HMP by monitoring the ν_1 and A-X absorptions as a function of time (0–1000 μ s) after HO₂ formation. The formation kinetics were measured as a function of [HO₂] in order to determine the rate constant $k_{\text{HO}_2+\text{HCHO}}$. The destruction kinetics were compared to a kinetics model to assess the quality of existing rate constants.

Methods

Apparatus and Chemicals

The cavity ringdown spectrometer, laser system, and gas kinetics flow cell have been described in detail in Chapter 2 (Figures 2.5, 2.7, 2.8), and only a brief summary of the mid-IR (MIR) and near-IR (NIR) configurations is presented here.

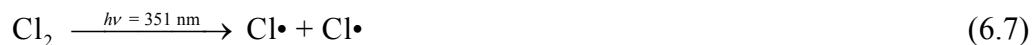
Tunable MIR light used to measure kinetics via the ν_1 absorption of HMP was generated using an optical parametric amplifier. For 65 mJ of 532 nm light and 4–12 mJ of tunable red light (620–665 nm), 0.6–0.8 mJ of tunable infrared light was generated (2900–3800 cm⁻¹). The infrared light was sent into an optical cavity consisting of two

highly reflective mirrors (Los Gatos Research, 2.8 μm peak, $R = 99.98\%$). Ringdown traces were collected with a liquid nitrogen cooled InSb detector (Judson J10D-M204-R01M-60) connected to a voltage amplifier (Analog Modules 351A-3) and PC oscilloscope card (GageScope CS1450). 80 μs of ringdown data were collected per shot, and 16 ringdowns were collected and averaged before being fit. The first eighth of the ringdown lifetime was removed before the data were refit in order to eliminate errors caused from noise near the peak of the ringdown.

Tunable NIR light used to measure kinetics via the A-X absorptions of HMP (6900–8500 cm^{-1} , 100 $\mu\text{J}/\text{pulse}$) was generated by sending the output from a Nd:YAG (532 nm, 370 mJ/pulse) pumped dye laser (DCM, Rh 640, or Rh 610 dye, 590–660 nm, 40 mJ/pulse peak) into a H_2 filled Raman shifter. The infrared light was sent into an optical cavity consisting of two highly reflective mirrors (Los Gatos Research, 1.35 or 1.20 μm peak, $R = 99.98\%$ or 99.99%). Ringdown traces were collected with an amplified InGaAs detector (ThorLabs PDA400) connected to a PC oscilloscope card (GageScope CS1450). 80 μs of ringdown data were collected per shot, and 16 ringdowns were collected and averaged before being fit. The first 1/20 of the ringdown lifetime was removed before the data were refit in order to eliminate errors caused from noise near the peak of the ringdown.

The hydroxymethylperoxy radicals ($\text{HOCH}_2\text{OO}\cdot$, HMP) measured in this experiment were generated by photolysis of Cl_2 in the presence of HCHO and O_2 (Reactions 6.7-6.9 and 6.1). Photolysis was initiated by 351 nm light from the excimer laser described in Chapter 2. The absorption cross section of Cl_2 at 351 nm is $\sigma_{351\text{nm}} = 1.9 \times 10^{-19} \text{ cm}^2 \text{ molec}^{-1}$.²⁷ For the MIR experiments, the UV flux was kept at 1.8×10^{17}

molec cm⁻³, resulting in 3.2% of the Cl₂ being photolyzed. For the NIR experiments, the UV flux was kept at 4.4×10^{17} photons cm⁻², resulting in 8.0% of the Cl₂ being photolyzed.



Cl₂ was introduced to the cell from a gas cylinder consisting of 3.5% Cl₂ in He (Air Liquide or Matheson Tri-Gas). HCHO was introduced to the cell by flowing N₂ gas through a vessel of paraformaldehyde (Sigma-Aldrich, 95%) heated to 110 °C. Heating paraformaldehyde leads to the formation of HCHO monomers and oligomers. To trap the oligomers, the N₂/HCHO gas was sent to a dry ice/acetone trap before being sent to the CRDS cell. This method was verified to produce a consistent [HCHO] ($\pm 10\%$ between experiments) as measured by the 2v₂ R branch (3510–3520 cm⁻¹)⁴⁰ and A-X bands (300–310 nm).¹¹⁶

Experimental and Flow Conditions

In our experiments, [HCHO] was factor of 30–1000 higher than [HO₂], with [HCHO] = 1×10^{17} molec cm⁻³ and [HO₂] = (1–30) $\times 10^{14}$ molec cm⁻³. We showed in Chapter 4 that by keeping [HCHO]:[HO₂] high, our v₁ spectrum is relatively free of interference from H₂O₂. Higher [HO₂] was required in the NIR in order to generate the higher [HMP] necessary to make measurements via the weak A-X bands (Chapter 4).

Kinetics measurements were made by keeping the spectrometer at a constant frequency and varying the photolysis-probe delay time over the range 0–1000 μs . As shown in the *Results* section, only the first 50 μs of data were used in the MIR (ν_1) experiment due to interference from other species at longer times (HMHP, HCOOH, H₂O₂). The entire range of photolysis-probe times was used for the NIR (A-X) experiment.

The experimental conditions for the HMP kinetics experiments are summarized in Table 6.1. Gas flows were measured using the flowmeters discussed in Chapter 2. The temperature of the gas kinetics cell was taken to be room temperature: no temperature control of any kind was attempted.

Table 6.1. Experimental conditions (gas flows, photolysis parameters, chemical concentrations, and spectrometer performance) for HMP kinetics experiments

	HMP, ν_1 (MIR)	HMP, A-X (NIR)
N ₂ Purge Flow – Left Mirror	450 sccm	450 sccm
N ₂ Purge Flow – Right Mirror	450 sccm	450 sccm
N ₂ /HCHO Flow	250 sccm	250 sccm
3.5% Cl ₂ / He Flow	14–70 sccm	170 sccm
N ₂ Dilution Flow	1250 sccm	1250 sccm
O ₂ Flow	650 sccm	650 sccm
Cell Pressure	300 torr	330 torr
Temperature (room)	293 ± 2 K	293 ± 2 K
Flush Time	30 ms	25 ms
Photolysis Window Length	5 cm	5 cm
Excimer Energy at 351 nm	160 ± 10 mJ/pulse	160 ± 10 mJ/pulse
% Cl ₂ Photolyzed	3.2%	8.0%
[Cl•] ₀ ~ [HO ₂] ₀	(1–5) × 10 ¹⁴ cm ⁻³	3 × 10 ¹⁵ cm ⁻³
[HCHO]	1 × 10 ¹⁷ cm ⁻³	1 × 10 ¹⁷ cm ⁻³
[O ₂]	2.0 × 10 ¹⁸ cm ⁻³	2.2 × 10 ¹⁸ cm ⁻³
Optical Cell Length	52 cm	52 cm
1/ τ_0 (purge only)	1.3 × 10 ⁵ Hz, 3638 cm ⁻¹	1.2 × 10 ⁵ Hz, 7550 cm ⁻¹
1/ τ (background gases)	1.4 × 10 ⁵ Hz, 3638 cm ⁻¹	1.3 × 10 ⁵ Hz, 7550 cm ⁻¹
$\Delta t/\tau^a$	0.34%	0.28%
Sensitivity (2 σ)	2.1 ppm Hz ^{-1/2}	1.6 ppm Hz ^{-1/2}

a) $\Delta t/\tau$ reported for averaging 16 ringdown traces per point

The cell flush time, [Cl₂], and [Cl•] are calculated from the experimental parameters in Table 6.1. Derivations of these equations are presented in Chapter 8; therefore, only the final results are presented here. The flush time is defined as the amount of time to remove the chemicals within the photolysis length from the ringdown cavity, and is calculated from Equation 6.10:

$$t_{flush} = \left(\frac{V_{in-out}}{\sum_{flush} f_i} \right) \times \left(\frac{p_{cell}}{p_{st}} \right), \quad (6.10)$$

where t_{flush} is the flush time for the chemical sample, V_{in-out} is the volume between the inlet for butyl nitrite and vacuum outlet ($V_{in-out} = 3.93 \text{ cm}^3$ for the cell used in these

experiments), $\sum_{flush} f_i$ is the total flow rate of gases in the direction of flushing (in sccm),

p_{cell} is the pressure in the CRDS cell, and p_{st} is the standard pressure (760 torr).

The fraction of Cl_2 that is photolyzed can be calculated from Equation 6.11:

$$\%_{photolysis} = \frac{\left(\frac{P_{excimer}}{A_{meter}} \right)}{F_{excimer}} \left(\frac{\lambda}{hc} \right) (\sigma_{Cl_2, \lambda}) (X) \left(\frac{A_{UV, laser}}{A_{UV, CRDS}} \right), \quad (6.11)$$

where $\%_{photolysis}$ is the fraction of RONO that is photolyzed, $(P_{excimer}/A_{meter})$ is the power per unit area of the UV light (read directly from the power meter), $F_{excimer}$ is the repetition rate of the excimer laser (10 Hz), h is Planck's constant, c is the speed of light, λ is the wavelength of the excimer light (351 nm), $\sigma_{Cl_2, \lambda}$ is the absorption cross section of Cl_2 at the excimer wavelength ($1.9 \times 10^{-19} \text{ cm}^2 \text{ molec}^{-1}$ at 351 nm), X is the quantum yield for photolysis (taken to be 1), $A_{UV, laser}$ is the area of excimer beam measured at the excimer laser output, and $A_{UV, CRDS}$ is the area of excimer beam measured at the CRDS cell. For

the ν_1 experiment, $\frac{A_{UV, laser}}{A_{UV, CRDS}} = 2$. For the A-X experiment, $\frac{A_{UV, laser}}{A_{UV, CRDS}} = 5$.

Results

We present the results of our kinetics study in four parts. First, we analyze the kinetics of $HO_2 + HCHO$ to derive an equation for the rate constant k_{HO_2+HCHO} based on our CRDS measurements. Second, we show the kinetics of HMP formation using the ν_1 band. In this part, we derive k_{HO_2+HCHO} . We also show that at long times, absorbance in the ν_1 region remains constant despite formation of $HCOOH$, indicating that the ν_1 band of HMP cannot be used to measure its destruction rate. Third, we show the kinetics of

HMP as measured by the A-X band. These results clearly show the destruction of HMP, and we derive a lifetime of HMP under our experimental conditions. In the *Discussion* section, we compare our results to the existing kinetic rate constants and our kinetics model. Our results are in excellent agreement with the literature, indicating that secondary chemistry and spectral interferences were well modeled in the previous studies.

Predicted HO₂ + HCHO Kinetics

At the beginning of our experiment (<100 μs), we have very fast conversion of Cl• to HO₂ (see the analysis from Chapter 4). Thus, we only need to be concerned with two reactions: HO₂ + HCHO (Reaction 6.1) and HO₂ self-reaction (Reaction 6.12)



where (+M) indicates that there are bimolecular and termolecular pathways.

We would like to derive an expression for how [HMP] will vary in time as a function of known parameters ([HCHO]₀, [HO₂]₀). The differentiated rate law for [HMP] is

$$\frac{d[\text{HMP}]}{dt} = k_1 [\text{HO}_2][\text{HCHO}], \quad (6.13)$$

where k_1 represents the rate constant for Reaction 6.1 (HO₂ + HCHO). Since we have chosen to use a large excess of [HCHO], we can reduce Equation 6.13 to a pseudo-first-order kinetics equation:

$$\frac{d[\text{HMP}]}{dt} = k_{1,eff} [\text{HO}_2], \quad (6.14)$$

where $k_{1,eff} = k_1 \times [\text{HCHO}]$.

Although [HCHO] is constant, [HO₂] is not, and we must determine the time dependence of [HO₂]. HO₂ is consumed by Reactions 6.1 and 6.12. Define k_{12a} as the rate constant for HO₂ bimolecular self-reaction and k_{12b} as the rate constant for HO₂ termolecular self-reaction. Then the differentiated rate law for [HO₂] is

$$-\frac{d[\text{HO}_2]}{dt} = 2(k_{12a} + k_{12b}[\text{M}])[\text{HO}_2]^2 + k_{1,\text{eff}}[\text{HO}_2], \quad (6.15)$$

where the factor of 2 indicates that two HO₂ radicals are consumed during self-reaction.

Integrating Equation 6.15 and solving for [HO₂](t) gives us

$$[\text{HO}_2](t) = \frac{k_{1,\text{eff}}[\text{HO}_2]_0}{k_{1,\text{eff}}e^{k_{1,\text{eff}}t} + 2(e^{k_{1,\text{eff}}t} - 1)(k_{12a} + k_{12b}[\text{M}])[\text{HO}_2]_0}. \quad (6.16)$$

Substituting Equation 6.16 back into Equation 6.14 yields

$$\frac{d[\text{HMP}]}{dt} = \frac{k_{1,\text{eff}}^2[\text{HO}_2]_0}{k_{1,\text{eff}}e^{k_{1,\text{eff}}t} + 2(e^{k_{1,\text{eff}}t} - 1)(k_{12a} + k_{12b}[\text{M}])[\text{HO}_2]_0}. \quad (6.17)$$

Although Equation 6.17 looks complicated, we can make a few simplifications based on the order of magnitudes for each term. Table 6.2 summarizes the orders of magnitudes for each term in Equation 6.17 and the parameters used to obtain these estimates.

Table 6.2. Orders of magnitude for each term in Equation 6.17, assuming conditions for the v_1 experiment ($[\text{HO}_2]_0 = 10^{14}$ molec cm⁻³, [HCHO] = 10¹⁷ molec cm⁻³, [M] = 10¹⁹ molec cm⁻³).

Parameter / Term	Estimate
k_1 (298 K)	5.5×10^{-14} cm ³ s ⁻¹ molec ⁻¹ ^{25, 26}
$k_{1,\text{eff}} = k_1 \times [\text{HCHO}]$	5500 s ⁻¹
k_{12a} (298 K)	1.5×10^{-12} cm ³ molec ⁻¹ s ⁻¹
k_{12b} (298 K)	4.9×10^{-32} cm ⁶ molec ⁻² s ⁻¹
$k_{1,\text{eff}}^2[\text{HO}_2]_0$	3×10^{21} cm ³ molec ⁻¹ s ⁻²
$k_{1,\text{eff}}e^{k_{1,\text{eff}}t}$	7241 s ⁻¹ ($t = 50$ μs)
Series Approx. $k_{1,\text{eff}}e^{k_{1,\text{eff}}t} \approx k_{1,\text{eff}}(1 + k_{1,\text{eff}}t)$	7013 s ⁻¹ ($t = 50$ μs)
$2(e^{k_{1,\text{eff}}t} - 1)(k_{12a} + k_{12b}[\text{M}])[\text{HO}_2]_0$	126 s ⁻¹

To first order, the $2(e^{k_{1,eff}t} - 1)(k_{12a} + k_{12b}[M])[HO_2]_0$ term is negligible compared to the $k_{1,eff}e^{k_{1,eff}t}$ term (for the highest $[HO_2]_0 = 5 \times 10^{14}$ molec cm^{-3} , this term will still be less than 5% of $k_{1,eff}e^{k_{1,eff}t}$). We also note that replacing $k_{1,eff}e^{k_{1,eff}t}$ with its Taylor series $k_{1,eff}(1 + k_{1,eff}t)$ only gives a 3% error at 50 μs . Using this Taylor series, we simplify Equation 6.17 at small times to

$$\frac{d[HMP]}{dt} = k_{1,eff} \left(\frac{[HO_2]_0}{k_{1,eff}t + 1} \right), \quad (6.18)$$

with the caveat that Equation 6.18 only holds true for the v_1 experiment (small $[HO_2]_0$) at short times ($<100 \mu s$). Even with this caveat, Equation 6.18 predicts that the slope $\frac{d[HMP]}{dt}$ will have a small time dependence due to depletion of HO_2 .

We can solve Equation 6.18 for $k_{1,eff}$, and then obtain k_1 :

$$k_{1,eff} = \frac{d[HMP]/dt}{[HO_2]_0 - \left(d[HMP]/dt \right) t}, \quad (6.19)$$

$$k_1 = \frac{d[HMP]/dt}{[HCHO] \left([HO_2]_0 - \left(d[HMP]/dt \right) t \right)}. \quad (6.20)$$

We cannot eliminate the $\left(\frac{d[\text{HMP}]}{dt}\right)t$ term, as this term indicates how much

$[\text{HO}_2]$ has been depleted. Instead, we make the approximation

$$[\text{HO}_2]_0 - \left(\frac{d[\text{HMP}]}{dt}\right)t \approx [\text{HO}_2]_0 - \left(\frac{d[\text{HMP}]}{dt}\right)t_{\text{avg}}, \quad (6.21)$$

where t_{avg} is taken to be half of the times being fit. For example, if 50 μs worth of data

are used to obtain $\left(\frac{d[\text{HMP}]}{dt}\right)$, then $t_{\text{avg}} = 25 \mu\text{s}$. By making this substitution, we

obtain the relation between k_1 and our kinetics data:

$$k_1 = \frac{\frac{d[\text{HMP}]}{dt}}{[\text{HCHO}] \left([\text{HO}_2]_0 - \left(\frac{d[\text{HMP}]}{dt}\right)t_{\text{avg}} \right)}. \quad (6.22)$$

Equation 6.22 would be the same equation obtained from a kinetics analysis assuming that HO_2 self-reaction (Reaction 6.12) is negligible. This is true for low $[\text{HO}_2]$, where Reaction 6.1 will dominate. At higher HO_2 , we cannot make these approximations, and the HO_2 dependence must be represented by Equation 6.17. This is yet another reason why k_1 cannot be well determined from the A-X experiment: $[\text{HO}_2]$ is much greater than in the ν_1 experiment.

Our derivation of Equation 6.22 has at least 10% error on the calculation of k_1 , due to the approximations made going from Equations 6.17 to 6.18, and the approximation made in Equation 6.21. However, this is likely of little consequence. Equation 6.22 depends on the absolute $[\text{HMP}]$, which requires knowledge of the absorption cross section σ to convert between absorbance and $[\text{HMP}]$. We are using absorption cross sections generated from relatively low levels of theory

(B3LYP/6-31+G(d,p)), and we expect much larger errors on the cross section ($> 20\%$) than from Equation 6.22.

Kinetics of HMP by ν_1 Absorption

Figures 6.1–6.4 show a series of kinetics traces for HMP measured at the two peaks of the ν_1 absorption band: 3610 cm^{-1} and 3630 cm^{-1} . We have already observed (Chapter 4) that these two regions are affected differently by interfering species (3610 cm^{-1} weakly by HCOOH , 3630 cm^{-1} by HOCH_2OOH , both by H_2O_2). By measuring the kinetics at both points of the ν_1 band, we can check that our measurements are invariant to the exact frequency used.

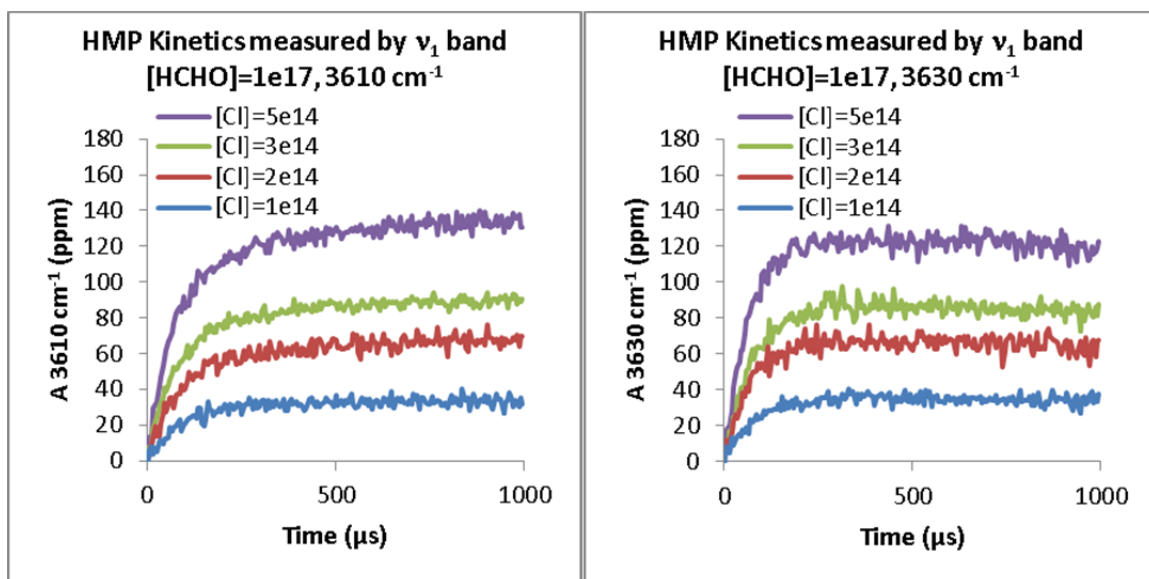


Figure 6.1. Kinetics traces of HMP using two frequencies within the ν_1 band: 3610 cm^{-1} (left) and 3630 cm^{-1} (right). Both plots were taken with $[\text{HCHO}] = 1 \times 10^{17}\text{ molec cm}^{-3}$, for $[\text{Cl}\cdot] = (1-5) \times 10^{14}\text{ molec cm}^{-3}$ (labeled on plots).

We note that the ν_1 absorbance scales with $[\text{Cl}\cdot]$ (and thus with $[\text{HO}_2]$), in accordance with Equation 6.13. We note that at long times (1 ms) where HMP is expected to be converted to other products, the ν_1 absorbance is remaining relatively

constant, despite an expected lifetime of HMP of at most 700 μs (Chapter 4, Table 4.2). This implies that side products or secondary products (H_2O_2 , HOCH_2OOH) are interfering with our HMP measurements at long times. Thus, we cannot use the ν_1 band to measure the kinetics of HMP destruction.

At short times, we have shown (Chapter 4) that the measured spectrum should be representative of HMP. Figure 6.2 shows the kinetics traces of HMP over the first 75 μs after HO_2 formation, as measured by the ν_1 band. Over this time range, we clearly observe pseudo-first-order kinetics effects within the first 50 μs : the growth of HMP is linear, with higher growth rates observed for higher $[\text{HO}_2]$. We also observe slight curvature beyond 50 μs , implying the loss of our pseudo-first-order kinetics conditions (likely due to $[\text{HO}_2]$ variance)

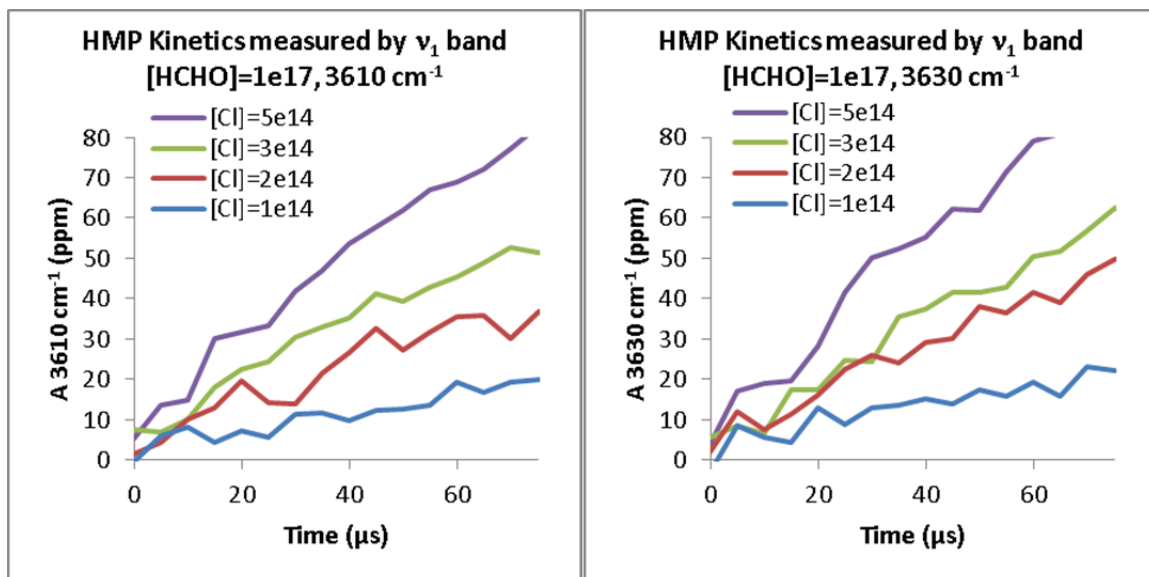


Figure 6.2. Kinetics traces of HMP over the first 75 μs of reaction, measured at 3610 cm^{-1} (left) and 3630 cm^{-1} (right). Both plots were taken with $[\text{HCHO}] = 1 \times 10^{17}$ molec cm^{-3} , for $[\text{Cl}\cdot] = (1-5) \times 10^{14}$ molec cm^{-3} (labeled on plots).

The kinetics data in Figures 6.1 and 6.2 are our raw spectroscopic data, and are presented in terms of absorbance. In order to calculate rate constants, we must convert

these data to absolute [HMP] using the absorption cross sections calculated in Chapter 4. For the two frequencies reported here, $\sigma_{\text{HMP},3610} = 1.3 \times 10^{-19} \text{ cm}^2 \text{ molec}^{-1}$ and $\sigma_{\text{HMP},3630} = 1.5 \times 10^{-19} \text{ cm}^2 \text{ molec}^{-1}$. These values are taken to be the average of the cross sections obtained by theoretical calculations (B3LYP/6-31+G(d,p)) and derived [HMP] from our kinetics model. These theoretical cross sections should be considered to have at least 20% uncertainty.

Using these cross sections, we can plot [HMP] vs time over 1 ms (Figure 6.3) and 75 μs , the range useful for calculating k_1 (Figure 6.4). At short times, we note that both bands are in excellent agreement with respect to [HMP] vs time, indicating very little interference from secondary products on short timescales. Over a 1 ms timescale, we note that the 3610 cm^{-1} measurements predict larger [HMP] than the 3630 cm^{-1} measurements for all $[\text{HO}_2]$, another indication that secondary species are causing spectral interference at longer times.

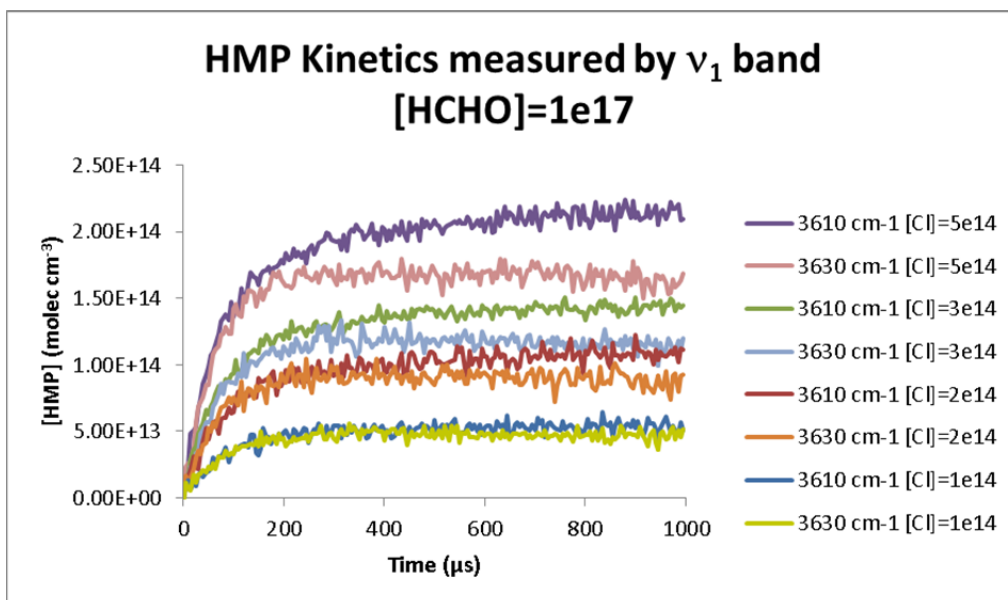


Figure 6.3. [HMP](t) measured by the ν_1 band (3610 cm^{-1} , 3630 cm^{-1}) for $[\text{Cl}\cdot] = (1-5) \times 10^{14} \text{ molec cm}^{-3}$. All data were taken with $[\text{HCHO}] = 1 \times 10^{17} \text{ molec cm}^{-3}$. Absolute [HMP] were calculated from absorbance data assuming $\sigma_{\text{HMP},3610} = 1.3 \times 10^{-19} \text{ cm}^2 \text{ molec}^{-1}$ and $\sigma_{\text{HMP},3630} = 1.5 \times 10^{-19} \text{ cm}^2 \text{ molec}^{-1}$.

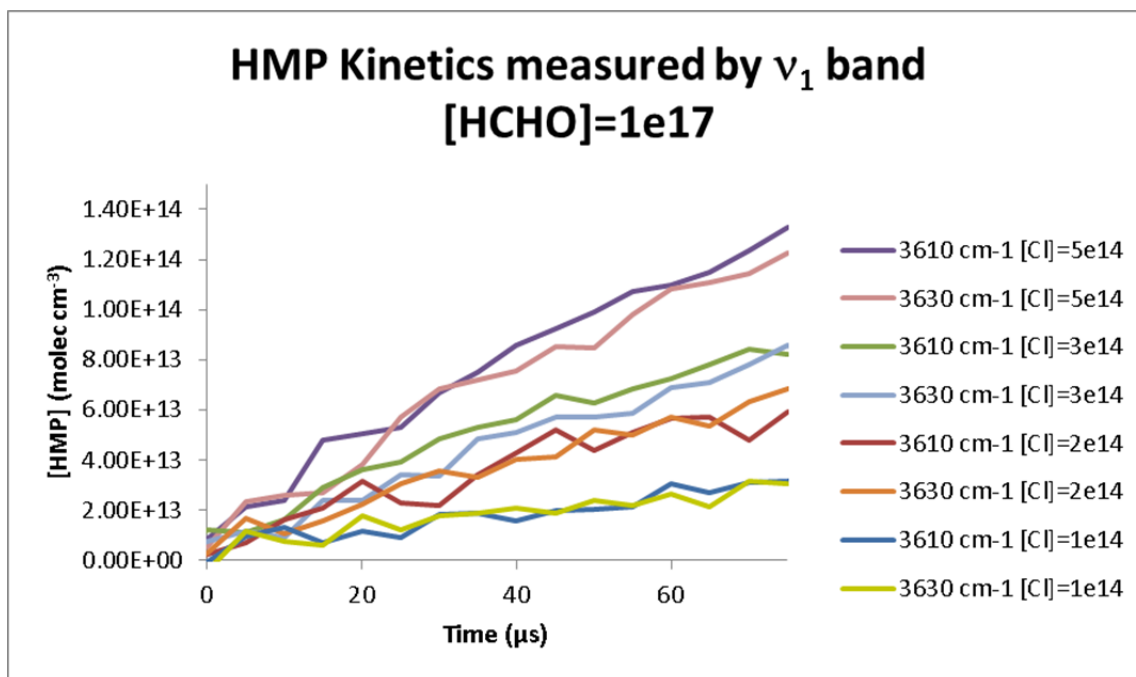


Figure 6.4. $[\text{HMP}](t)$ at short times ($75 \mu\text{s}$), measured by the ν_1 band (3610 cm^{-1} , 3630 cm^{-1}) for $[\text{Cl}\cdot] = (1-5) \times 10^{14} \text{ molec cm}^{-3}$. All data were taken with $[\text{HCHO}] = 1 \times 10^{17} \text{ molec cm}^{-3}$. Absolute $[\text{HMP}]$ were calculated from absorbance data assuming $\sigma_{\text{HMP},3610} = 1.3 \times 10^{-19} \text{ cm}^2 \text{ molec}^{-1}$ and $\sigma_{\text{HMP},3630} = 1.5 \times 10^{-19} \text{ cm}^2 \text{ molec}^{-1}$.

Given the data in Figure 6.4, we can calculate k_1 using Equation 6.22. These results are summarized in Table 6.3. We use only the absorption data within the first $50 \mu\text{s}$ of reaction to ensure that we still have pseudo first order conditions, and that the errors introduced from the approximations used to derive Equation 6.22 do not become too large.

Table 6.3. Determination of k_1 from CRDS ν_1 absorption data and Equation 6.22 (main text), $[\text{HCHO}] = 1 \times 10^{17} \text{ molec cm}^{-3}$, $t_{\text{avg}} = 25 \mu\text{s}$ ($50 \mu\text{s}$ of data used for determining $d[\text{HMP}]/dt$).

$\bar{\nu}$ (cm^{-1})	3610	3610	3610	3610	3630	3630	3630	3630
$[\text{HO}_2]_0$ (cm^{-3})	1e14	2e14	3e14	5e14	1e14	2e14	3e14	5e14
$d[\text{HMP}]/dt$ ($\text{cm}^{-3} \text{ s}^{-1}$)	3.3e17	8.8e17	1.2e18	1.8e18	4.3e17	8.8e17	1.1e18	1.7e18
k_1 ($\text{cm}^3 \text{ s}^{-1}$)	4.0e-14	5.7e-14	5.0e-14	4.4e-14	5.4e-14	5.6e-14	4.6e-14	4.0e-14

If we simply average the individual k_1 obtained from our data, we **obtain** $k_1 = (4.8 \pm 1.7) \times 10^{-14} \text{ cm}^3 \text{ molec}^{-1} \text{ s}^{-1}$ (**2 σ error**). The uncertainty on this rate constant includes the scatter of the k_1 data, 20% uncertainty on the IR absorption cross section of HMP and 10% uncertainty on k_1 due to the approximations made to obtain Equation 6.22.

Kinetics of HMP by A-X Absorption

As explained in the *Introduction*, our kinetics measurements using the A-X bands are well suited to measure HMP destruction, and therefore the lifetime of HMP in our experiment. While we were able to derive an accurate ($\pm 20\%$) expression for the rate constant of HMP formation, we cannot do the same for destruction of HMP for two reasons. First, destruction of HMP occurs by multiple pathways (Reactions 6.2–6.6). We cannot determine individual destruction rate constants; rather, we can only examine the overall destruction of HMP. Second, we observe that Reactions 6.3 and 6.6 regenerate HO_2 , restarting the $\text{HO}_2 + \text{HCHO}$ reaction. Therefore, the lifetime of HMP will be greater than a simple analysis of the rate constants of HMP destruction.

While we cannot extract exact rate constants, we are able to examine multiple A-X bands to determine whether or not the overall HMP decay kinetics are consistent between bands. These results can also be used in conjunction with a kinetics model to determine whether our data support or refute the existing HMP rate constants (*Discussion section*).

Figure 6.5 shows the kinetics of [HMP] as measured by the A-X bands at 7561 cm^{-1} and 7557 cm^{-1} (on and off peak of the 15_0^1 transition) and 7386 cm^{-1} (off peak of

the 0_0^0 transition). All absorbances have been converted to [HMP] via the absorption cross sections determined in Chapter 4.

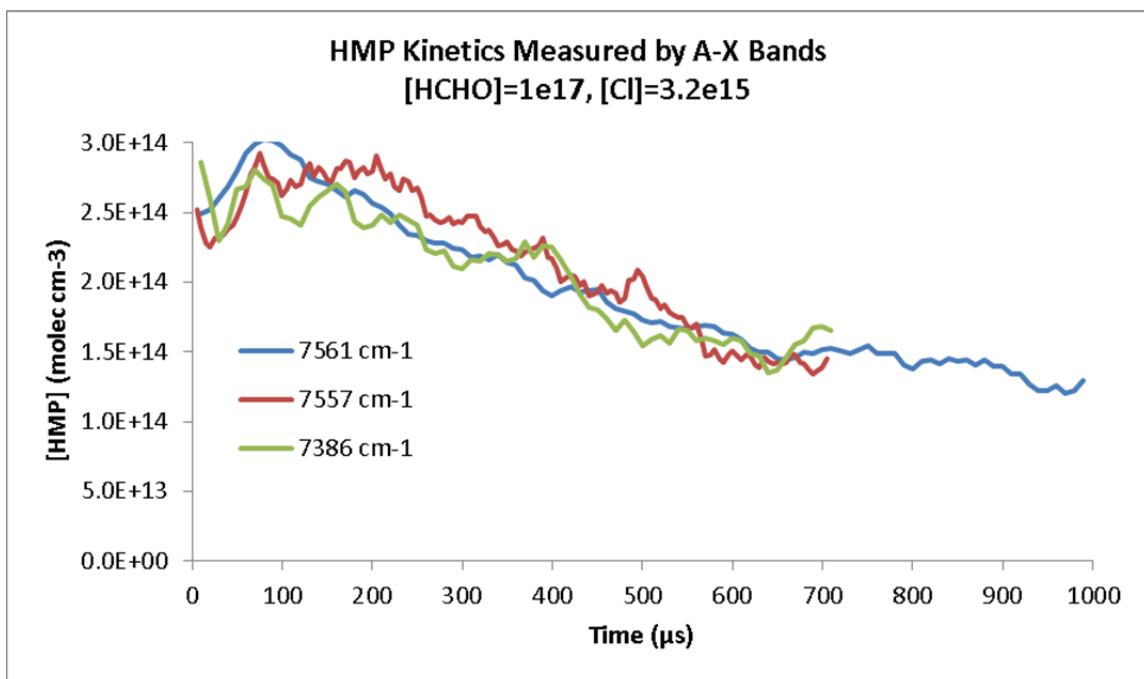


Figure 6.5. Kinetics traces of HMP using three frequencies within the A-X bands: 15_0^1 (peak 7561 cm^{-1} and off-peak 7557 cm^{-1}) and 0_0^0 (off-peak 7386 cm^{-1}). All data were taken with $[\text{HCHO}] = 1 \times 10^{17}\text{ molec cm}^{-3}$, $[\text{Cl}\cdot] = 3.2 \times 10^{15}\text{ molec cm}^{-3}$.

We observe excellent agreement in the calculation of [HMP] across the three measured frequencies. In all cases, we observe [HMP] reaching its maximum in the range 100–200 μs (error due to the noise in the kinetics traces). At 1 ms, we observe 41% of the maximum [HMP] in our system, implying a lifetime of HMP slightly longer than 1 ms for our experimental conditions.

The observed lifetime ($>1\text{ ms}$) is much larger than the “estimated” lifetimes from Chapter 4, Table 4.2 (75 μs). This is simply because the lifetimes in Chapter 4 were calculated by assuming $[\text{HO}_2]$ was at its maximum value throughout the experiment, an invalid assumption for the A-X conditions where $[\text{HO}_2]$ is high, but consumed by both

HO₂ + HCHO (Reaction 6.1) and self-reaction (Reaction 6.12). We should not be surprised that the actual lifetime of HMP is an order of magnitude greater than our relatively simple analysis.

Discussion

Comparison of HO₂ + HCHO Kinetics Results (ν₁) to Literature

Using the kinetics data obtained by measuring the ν₁ absorbance of HMP, we were able to calculate a 298 K rate constant for HO₂ + HCHO of $k_1 = (4.8 \pm 1.7) \times 10^{-14} \text{ cm}^3 \text{ molec}^{-1} \text{ s}^{-1}$. We compare this value to previous measurements in Table 6.4. Our value is in excellent agreement with the literature,^{96, 99} particularly the studies by Veyret and Burrows that directly detected HMP via its B-X absorption in the UV.^{25, 26} The current NASA/JPL Data Evaluation²⁷ recommends a rate of $5 \times 10^{-14} \text{ cm}^3 \text{ molec}^{-1} \text{ s}^{-1}$ with a factor of 5 uncertainty: we recommend the same rate constant with only 40% uncertainty.

Table 6.4. Comparison of rate constant $k_{\text{HO}_2+\text{HCHO}}$ to literature values.

Ref	$k_{\text{HO}_2+\text{HCHO}}$ (298 K) ($10^{-14} \text{ cm}^3 \text{ molec}^{-1} \text{ s}^{-1}$)	Molecule Detected	Method	Pressure (torr)
This work	4.8 ± 1.7	HOCH ₂ OO•, ν ₁	PLP-IR-CRDS, slow flow	300
Veyret, Burrows, 1989 ^{25, 26}	6.2 (factor of 5)	HOCH ₂ OO•, B-X	Flash Photolysis, slow flow, UV Absorption	85-170
Su, 1979 ⁹⁹	1.0 (order of magnitude)	HCOOH, H ₂ O ₂ , HOCH ₂ OOH	Photolysis, FTIR	700
Barnes, 1985 ⁹⁶	11 ± 4 (273 K) ^a	HOCH ₂ OONO ₂ , HNO ₄	Flash photolysis, FTIR	400
JPL/NASA ²⁷	5.0 (factor of 5)	N/A	Recommendation	N/A

a) Using Veyret's temperature dependence of $\exp[625/T]$, Barnes's rate constant is equivalent to $k_1(298\text{K}) = (9.1 \pm 3.3) \times 10^{-14} \text{ cm}^3 \text{ molec}^{-1} \text{ s}^{-1}$.

Comparison of HMP Destruction Kinetics (A-X) to Existing Model

The kinetics measurements made via the A-X predict an overall lifetime for HMP of slightly greater than 1 ms under our conditions ($[\text{HO}_2] = 3 \times 10^{15} \text{ molec cm}^{-3}$, $[\text{HCHO}] = 1 \times 10^{17} \text{ molec cm}^{-3}$). Because of the multiple destruction pathways of HMP and regeneration of HO_2 (Reactions 6.2-6.6), it is difficult to estimate whether or not this lifetime is reasonable. Instead, we compare our results to a kinetics model based on rate constants taken from the literature.^{27, 117, 118} Regarding HMP formation, we run our model using both Veyret's rate constant, $k_{1,298\text{K,Veyret}} = 6.3 \times 10^{-14} \text{ cm}^3 \text{ molec}^{-1} \text{ s}^{-1}$,²⁶ and the NASA/JPL recommendation, $k_{1,298\text{K,JPL}} = 5.0 \times 10^{-14} \text{ cm}^3 \text{ molec}^{-1} \text{ s}^{-1}$.²⁷ Our model is presented in Appendix E; here, we show only the results of the modeling.

We compare our A-X CRDS kinetics results to the model in Figure 6.6. Two plots are shown: absolute [HMP] (left), and the relative concentration $[\text{HMP}]/[\text{HMP}]_{\text{max}}$ (right). For clarity, we only show the kinetics as measured at 7561 cm^{-1} . This measurement carries two advantages: it is the strongest absolute absorbance measured, and there is no background H_2O that adds to the spectrometer noise in this region. We have already shown that the kinetics measurements at 7557 and 7386 cm^{-1} give similar results (Figure 6.5): therefore, the comparison in Figure 6.6 is generally valid across the A-X bands measured.

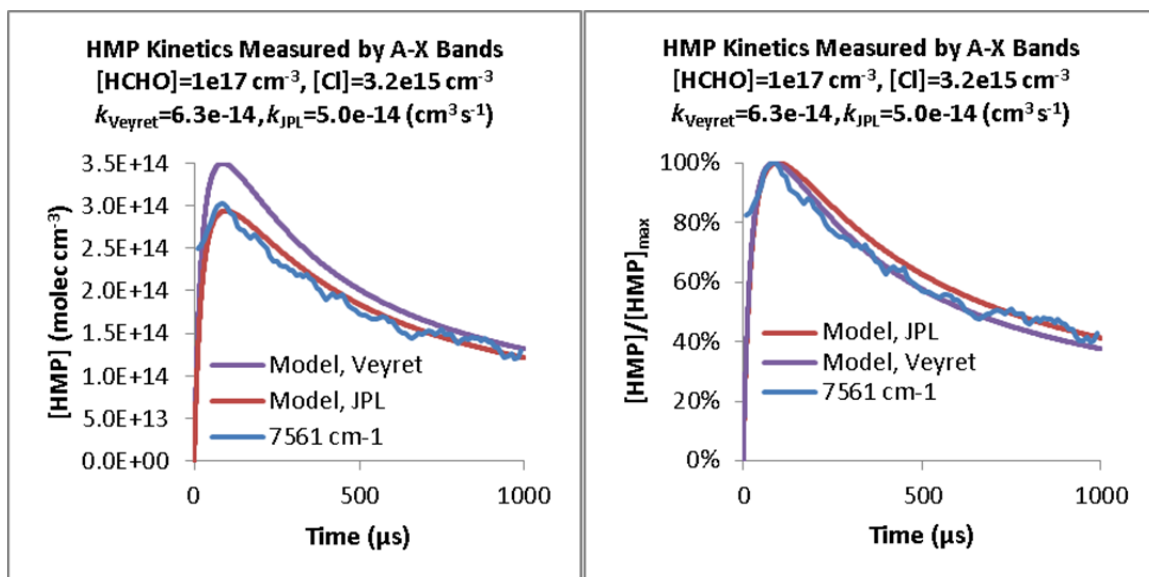
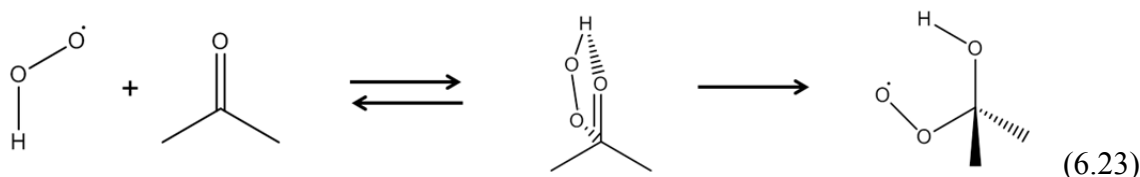


Figure 6.6. [HMP] (left) and the relative concentration $[\text{HMP}]/[\text{HMP}]_{\text{max}}$ (right), as experimentally measured (blue, CRDS A-X band) and modeled (purple and red). The purple curve uses Veyret's rate constant for $k_{\text{HO}_2+\text{HCHO}}$,²⁶ while the red curve uses the NASA/JPL data evaluation's recommendation.²⁷

The plots in Figure 6.6 show excellent agreement between our measured kinetics and the existing models. The absolute [HMP] predicted using either rate constant agrees within $\pm 25\%$. However, due to the large errors on the absorption cross section, this agreement may be accidental. The more significant data are the relative concentrations $[\text{HMP}]/[\text{HMP}]_{\text{max}}$. Regardless of the exact $k_{\text{HO}_2+\text{HCHO}}$ used, the models are in near perfect agreement with our data, predicting HMP lifetimes of 1 ms under our experimental conditions. Our data cannot differentiate between the individual destruction rate constants (Reactions 6.2–6.5); however, the agreement between model and experiment suggest that the sum of HMP destruction rates in the literature^{25, 26, 99} is quite accurate.

Application of Our Kinetics Methods to HO₂ + Acetone

As stated in Chapter 4, the “holy grail” of the HO₂ + carbonyl studies is direct detection of the isomerization product of HO₂ + acetone: 2-hydroxyisopropylperoxy (2-HIPP, Reaction 6.23).



Current experimental studies measuring show that HO₂ is consumed faster than expected (self-reaction) when acetone is present.²³ Because this study only detects [HO₂], it is not able to determine whether isomerization to 2-HIPP is taking place or if a Chaperone mechanism is causing a rate enhancement of the self-reaction.

The CRDS methods developed in Chapters 4-6 provide a method for direct detection and kinetics measurements of 2-HIPP. If we can obtain ν_1 and A-X spectra of 2-HIPP, then we will be able to measure its formation and destruction kinetics in a similar manner as we have done with HMP. Below, we provide an analysis of the experimental requirements for CRDS detection and kinetics measurements on 2-HIPP.

Since our detection method is spectroscopic in nature, we must first determine how the absorption cross sections of 2-HIPP compare to HMP. We can estimate the ν_1 cross section using quantum chemistry (B3LYP/6-31+G(d,p)) and compare to the cross section of HMP. At this level of theory, we obtain $\int \sigma_{\nu_1, 2\text{-HIPP}} d\bar{\nu} = 47 \text{ km mol}^{-1}$ and $\int \sigma_{\nu_1, \text{HMP}} d\bar{\nu} = 53 \text{ km mol}^{-1}$. To first order, we can assume that the absorption cross sections are equivalent. Regarding the A-X transition, the dipole moments of HMP and 2-HIPP are roughly equivalent, 2.1 debye for HMP, 2.2 debye for 2-HIPP at

B3LYP/6-31+G(d,p), with the magnitudes remaining constant between the A and X states. The dipole derivative is solely based on the change in direction of the π^* orbital on the O-O group, which is also the same between 2-HIPP and HMP. Finally, the potential energy surfaces in Chapter 5 show that both 2-HIPP and HMP have 3 deep torsional minima, and we should expect to see a series of bandheads much like HMP. A crude estimate of the strength of the 2-HIPP A-X bandheads is that they will be as strong as HMP. **Taken as a whole, this means that our goals are to generate nearly as much 2-HIPP as we did HMP.** Based on Figures 6.3 and 6.5, we should be able to make measurements of 2-HIPP kinetics for $[2\text{-HIPP}] = 10^{13}$ molec cm^{-3} (v_1) experiment and 10^{14} molec cm^{-3} (A-X) experiment.

Next, consider the equilibrium (K_{eq}) and rate constants (k) for Reaction 6.23. There are currently three estimates of these constants: Hermans et al. (theory),¹⁹ Cours et al. (theory),²² and Grieman et al. (experiment).²³ The literature values are summarized in Tables 6.5 and 6.6. Hermans reports a temperature dependent equation for both K_{eq} and k : these equations are entered into the tables. Cours's and Grieman's studies do not report such equations, instead reporting K_{eq} and k for selected temperatures. Here, we fit these data over the range 200-300 K to aid in further analysis. These fits and 298 K rate constants are reported below.

Table 6.5. Equilibrium constants for HO₂ + acetone, from theory (Hermans, Cours) and experiment (Grieman), and for HO₂ + HCHO (Hermans). Temperature-dependent equations for Cours and Grieman were obtained by a fit to their data.

Ref	K_{eq} HO ₂ + Acetone (cm ³)	K_{eq} HO ₂ +HCHO (cm ³)	Ratio (Acetone/HCHO)
Hermans ¹⁹	$7.81 \times 10^{-28} \exp\left[\frac{7201}{T}\right]$ (2.44×10^{-17} at 298 K)	$4.44 \times 10^{-27} \exp\left[\frac{8007}{T}\right]$ (2.07×10^{-15} at 298 K)	$0.176 \times \exp\left[\frac{-806}{T}\right]$ (0.012 at 298 K)
Cours ²²	$1.14 \times 10^{-29} \exp\left[\frac{6085}{T}\right]$ (8.64×10^{-21} at 298 K)		
Grieman ²³	$2.88 \times 10^{-24} \exp\left[\frac{3961}{T}\right]$ (1.58×10^{-18} at 298 K)		

Table 6.6. Rate constants for HO₂ + acetone from theory (Hermans, Cours) and for HO₂ + HCHO (Hermans). Temperature-dependent equations for Cours were obtained by a fit to their data.

Ref	k HO ₂ + Acetone (cm ³ s ⁻¹)	k HO ₂ + HCHO (cm ³ s ⁻¹)	Ratio (Acetone/HCHO)
Hermans ¹⁹	$4.98 \times 10^{-15} \exp\left[\frac{1460}{T}\right]$ (6.68×10^{-13} at 298 K)	$5.68 \times 10^{-15} \exp\left[\frac{1209}{T}\right]$ (3.28×10^{-13} at 298 K)	$0.878 \times \exp\left[\frac{251}{T}\right]$ (2.04 at 298 K)
Cours ²²	$4.07 \times 10^{-16} \exp\left[\frac{-47}{T}\right]$ (3.49×10^{-16} at 298 K)		

We note that the equilibrium constants for HO₂ + acetone are much lower than for HO₂ + HCHO. At best (Hermans's calculation), K_{eq} for HO₂ + acetone is a factor of 100 less than HO₂ + HCHO. At worst (Cours), the difference is a factor of 10⁶. Grieman's experiment splits the middle of these studies. In order to observe 2-HIPP, we must reduce the temperature of our system such that K_{eq} of HO₂ + acetone is at least equal to our room temperature K_{eq} of HO₂ + HCHO.

Using the K_{eq} in Table 6.5, we must reduce the temperature of our system to 250 K (Hermans), 185 K (Cours), or 195 K (Grieman) in order to obtain K_{eq} =

$2.1 \times 10^{-15} \text{ cm}^3$, the same equilibrium constant that we attained for our $\text{HO}_2 + \text{HCHO}$ experiment. 250 K is accessible with the current CRDS apparatus (Chapter 2). However, modifications must be made to achieve temperatures below 200 K (in theory by improving the cell insulation and using liquid nitrogen as the coolant rather than dry ice/methanol).

Even once the $\text{HO}_2 + \text{acetone}$ complex is formed, we must now be concerned with how fast it will isomerize into 2-HIPP. Hermans's calculations (Table 6.6) imply that 2-HIPP formation has a rate constant equivalent to HMP formation. However, Cours's calculations disagree significantly, predicting 2-HIPP formation to be a factor of 1000 slower than HMP. If 2-HIPP formation is very slow, yet destruction of 2-HIPP is just as fast as HMP (analogous to Reactions 6.2–6.6), then we will observe very little 2-HIPP in our spectroscopy experiments, making kinetics measurements extremely difficult. However, if 2-HIPP formation is as fast HMP formation, then we should be able to make measurements on the kinetics of 2-HIPP, subject to the temperature control of our apparatus.

Conclusions

In this chapter, we have reported the kinetics of HMP formation (from $\text{HO}_2 + \text{HCHO}$) and destruction as measured by its ν_1 and A-X spectroscopic bands. The strong ν_1 band is a unique measure of HMP at short times, making it ideal for measurement of the $\text{HO}_2 + \text{HCHO}$ rate constant. The A-X bands are weaker, but are unique measures of HMP at long times, making them ideal for studying HMP destruction. We report a rate constant $k_{\text{HO}_2+\text{HCHO}} = (4.8 \pm 1.7) \times 10^{-14} \text{ cm}^3 \text{ molec}^{-1} \text{ s}^{-1}$ (2σ uncertainty)

on the basis of our ν_1 kinetics study. Our rate constant is in excellent agreement with previous reports and data evaluations, but with lower uncertainty.^{25-27, 96, 99} Under our experimental conditions for the A-X experiment ($[\text{HO}_2] = 3.2 \times 10^{15}$ molec cm^{-3} , $[\text{HCHO}] = 1 \times 10^{17}$ molec cm^{-3}), the lifetime of HMP was 1 ms, in excellent agreement with predictions made from our kinetics model consisting of rate constants from the literature.^{26, 27, 117, 118}

The spectroscopy, quantum chemistry, and kinetics results presented in Chapters 4–6 suggest that we can apply our methods to studying the $\text{HO}_2 + \text{acetone}$ reaction. We have made predictions regarding the ν_1 and A-X band positions for 2-HIPP (Chapter 5) and the experimental conditions (concentrations, temperatures) required to observe 2-HIPP in our apparatus (this chapter). Modification of our spectrometer to reach temperatures of 200 K or less should be sufficient to permit measurements of 2-HIPP.

Acknowledgements

We thank Andrew Mollner for assistance with obtaining the time dependent ν_1 spectra. The experiments performed in this chapter were funded under NASA Upper Atmosphere Research Program Grants NAG5-11657, NNG06GD88G, and NNX09AE21G2, California Air Resources Board Contract 03-333 and 07-730, National Science Foundation CHE-0515627, and a Department of Defense National Defense Science and Engineering Graduate Fellowship (NDSEG).